Journal of Oceanology and Limnology

https://doi.org/10.1007/s00343-026-5404-1

Research Paper

Spatiotemporal variability of surface particulate organic carbon distributions in the Yellow Sea: multi-temporal scale analysis and environmental controls*

Yujie SHENG[1], Chunli LIU[1, **], Bei SU[2, **], Qicheng MENG[3, 4], Muhsan Ali KALHORO[1, 5], Zhiyuan HE[1], Min LI[1]

[1] *Marine College, Shandong University, Weihai 264209, China*

[2] *Institute of Marine Science and Technology, Shandong University, Qingdao 266237, China*

[3] *State Key Laboratory of Satellite Ocean Environment Dynamics, Second Institute of Oceanography, Ministry of Natural Resources, Hangzhou 310012, China*

[4] *Observation and Research Station of Yangtze River Delta Marine Ecosystems, Ministry of Natural Resources, Zhoushan 316022, China*

[5] *Faculty of Marine Sciences, Lasbela University of Agriculture, Water and Marine Sciences, Uthal 90150, Pakistan*

Received Oct. 19, 2025; accepted in principle Dec. 4, 2025; accepted for publication Feb. 5, 2026

Abstract Particulate organic carbon (POC) is critical to the coastal carbon cycle of the Yellow Sea (YS), a typical marginal sea, but its interannual-to-multiyear variability and driving mechanisms remain unclear due to the limitations of traditional linear or single-factor analyses. To address this gap, we employed model-derived surface POC data from 2003 to 2023 and wavelet coherence analysis to investigate POC variability and regulating mechanisms at multi-scales in the YS. The dominant spatiotemporal mode of surface POC exhibits pronounced seasonality, a consistent coastal-offshore gradient (higher in coastal waters), and a spring maximum, which is regulated by the seasonal alternation controlled by coastal production or input and offshore stratification or ventilation. Wavelet analysis reveals distinct subregional differences in driving mechanisms of POC variability at interannual-to-multiyear scales. Colored dissolved organic matter (CDOM) is the optimal single driver in most subregions, while sea surface temperature (SST) dominates in the Southern Yellow Sea Cold Water Mass (SYSCWM). Specific optimal multi-factor combinations include CDOM+sea surface wind speed (SSW) in the Northern Yellow Sea Cold Water Mass (NYSCWM), chlorophyll *a* (Chl *a*)+Photosynthetically Available Radiation (PAR)+partial pressure of carbon dioxide (pCO$_2$) in the SYSCWM, CDOM+Chl *a*+suspended matter (SPM) in the Jiangsu Shoal (JSS) and CDOM+sea surface salinity (SSS) in the Changjiang River estuary (CRE). These findings clarify the subregional heterogeneity of POC variability and its driving mechanisms in the YS at interannual-to-multiyear scales, and provide a robust scientific basis for accurate regional carbon budget assessments and the optimization of marine numerical models.

Keyword: Yellow Sea; particulate organic carbon (POC); wavelet analysis; spatiotemporal variability; interannual-to-multiyear

1 INTRODUCTION

Against the backdrop of escalating atmospheric carbon dioxide (CO_2) concentrations, the ocean serves as a critical carbon sink, absorbing about 2.6± 0.6 Pg C/a and thereby exerting a moderating influence on global climate systems (Friedlingstein et al., 2019). Particulate organic carbon (POC) plays a central role in the “biological pump”, a collective set of processes that convert organic matter

* Supported by Key Research and Development Program of Hainan Province (No. ZDYF2023SHFZ173), the National Key Research and Development Program of China (Nos. 2023YFC3108104, 2020YFA0608304), the National Natural Science Foundation of China (No. 42230404), and the Natural Science Foundation of Shandong Province (No. ZR2020MD098)

** Corresponding authors: chunliliu@sdu.edu.cn; bei.su@sdu.edu.cn

produced in the surface layer into particles capable of sinking or being transported laterally (Honjo et al., 2014). These particles facilitate the transfer of carbon from the atmosphere to the deep-sea reservoirs, thereby sustaining the carbon sequestration capacity (Honjo et al., 2014; Heinze et al., 2015). As a key carrier and tracer of organic carbon in marine environments, surface POC integrates signals of both biological production (e.g., phytoplankton blooms) and physical redistribution (e.g., advection, mixing) (Yu et al., 2019). Consequently, elucidating the spatiotemporal variability of POC at seasonal and interannual scales, as well as its covariability with environmental drivers, is indispensable for interpreting variability in the ocean carbon sink and constraining regional carbon budgets.

Time series observations of surface POC consistently reveal two distinct temporal scales of variability, each characterized by unique drivers and spatial distributions. At the seasonal scale, pronounced seasonal variability is evident, marked by coherent springtime increases in surface POC concentrations and large fluctuations in coastal waters (Allison et al., 2010; Stramska and Bialogrodzka, 2016). These seasonal patterns are typically linked to phenological cycles of primary production, stratified water column conditions, and seasonal forcing (e.g., light availability, nutrient supply) (Stramska and Bialogrodzka, 2016). At the interannual-to-multiyear scales, basin-wide anomalies often superimpose on and disrupt the seasonal baseline; a prominent example is the 2013–2017 North Pacific warm anomaly, which altered surface POC dynamics across the entire basin (Yu et al., 2019). Such interannual variability is frequently associated with large-scale climate modes (e.g., El Niño-Southern Oscillation, Pacific Decadal Oscillation) that modulate sea temperature, ocean circulation, and nutrient availability (Yu et al., 2019). Importantly, when synthesizing data across offshore and coastal waters, surface POC signals exhibit substantial regional variability at the seasonal and interannual scales, underscoring the need for scale-aware analytical frameworks to avoid misinterpretation of cross-regional comparisons (Rouf et al., 2021).

The mechanisms governing POC dynamics differ systematically between offshore and coastal waters. In the offshore waters, surface POC variability is tightly coupled to primary production and particle transformation processes (e.g., aggregation, remineralization), while basin-scale advection and mixing processes dictate surface POC redistribution pathways and background concentration gradients (Stramski et al., 2022). In contrast, coastal waters exhibit more complex POC dynamics, shaped by interactions between local topography, coastal circulation, and shelf-specific processes (Liénart et al., 2017). Rouf et al. (2021) conducted a comprehensive review of these coastal-specific mechanisms, highlighting that the resuspension of benthic sediments and cross-shelf exchange processes drive both vertical and horizontal redistribution of surface POC. Meanwhile, seasonal water column stratification and cold water masses structure the vertical coupling between surface and subsurface layers and further induce heterogeneity of surface POC distributions (Bridier et al., 2021). Notably, in coastal waters influenced by river plumes, terrestrial inputs of colored dissolved organic matter (CDOM) and fine-grained particles, coupled with plume expansion and episodic resuspension events, usually modulate the magnitude of surface POC variability (Hong et al., 2021; Sun et al., 2024).

The Yellow Sea (YS), a representative marginal sea in the Northwest Pacific, exhibits particularly strong optical complexity and pronounced nonstationarity in surface POC dynamics, driven by a confluence of physical, biological, and terrestrial processes (Fan et al., 2018). Wei et al. (2019) developed a composite algorithm covering the Chinese seas (including the YS) by categorizing water types and selecting optimal optical proxies, which improves the accuracy of regional POC retrieval. Cai et al. (2022) subsequently proposed a hybrid model for the East China Sea integrating color index and empirical band ratio methods, applying tailored sub-algorithms via distinct spectral features to support long-term dynamic monitoring of POC. However, there remains a lack of regional algorithms for accurate POC retrieval in the YS. In addition, although previous studies have well characterized the seasonal dynamics and spatial distributions of POC in the YS (Fan et al., 2018; Tao et al., 2018; Wang et al., 2020; Guo et al., 2022), the interannual-to-multiyear variability of POC in the YS remains poorly understood. Previous analytical approaches, including primarily linear models and single-factor correlations (Fan et al., 2018; Seo et al., 2022), are inadequate to resolve specific periodic patterns or to quantify the synergistic effects and relative weights of combined controlling factors. Multivariate wavelet coherence (MWC) provides a joint time-frequency framework to quantify covariability among multi-drivers and map their scale- and phase-specific relationships, thereby uncovering evolving synergies between drivers and shifts in their relative roles across different temporal scales. Recent research has demonstrated the efficacy of MWC in resolving multivariate coupling and temporal stability within marine biogeochemical systems (Xu et al., 2025).

Therefore, this study evaluates covariability between surface POC and its primary environmental drivers across multiple temporal and spatial scales based on the MWC. Specifically, this study addresses three objectives: (i) develop and validate a region-specific retrieval algorithm for surface POC in the YS; (ii) characterize the spatial distribution patterns, seasonal cycles and interannual trends of surface POC during 2003–2023; and (iii) assess the covariability between surface POC and its primary environmental drivers in four subregions. This analysis not only quantifies seasonal to multiyear variability in POC and its linkages to environmental factors but also clarifies coastal-offshore contrasts in POC dynamics.

2 DATA AND METHOD

2.1 Study area

The study focuses on the YS (~31°N–41°N, 117°E–127°E), a semi-enclosed marginal shelf sea in the northwestern Pacific (Li et al., 2023). It covers ~3.8× 10^5 km^2 with a mean depth of ~44 m and shows pronounced seasonality (Wang et al., 2016). To systematically study the interannual-to-multiyear variation of surface POC and the mechanisms regulating it in the YS, four subregions were selected in the YS from north to south and from coastal to offshore according to geographical and hydrological characteristics of the YS and the location of the ocean front. Each region is defined by a 1°×1° rectangle box (Fig.1). The Northern Yellow Sea Cold Water Mass (NYSCWM; 37.75°N–38.75°N, 123.05°E–124.05°E) samples the northern Yellow Sea Cold Water Mass (YSCWM) transition area (Xia et al., 2019). The Southern Yellow Sea Cold Water Mass (SYSCWM; 35.25°N–36.25°N, 124.00°E–125.00°E) represents a strongly stratified cold-core regime in summer (Yu et al., 2022). The Changjiang River estuary (CRE; 30.50°N–31.50°N, 123.50°E–124.50°E) reflects buoyant, sediment- and CDOM-rich conditions (Chen et al., 2024). The Jiangsu Shoal (JSS; 32.70°N–33.70°N, 121.50°E–122.50°E) is a tide- and bathymetry-dominated high-turbidity belt with persistent resuspension (Su et al., 2017).

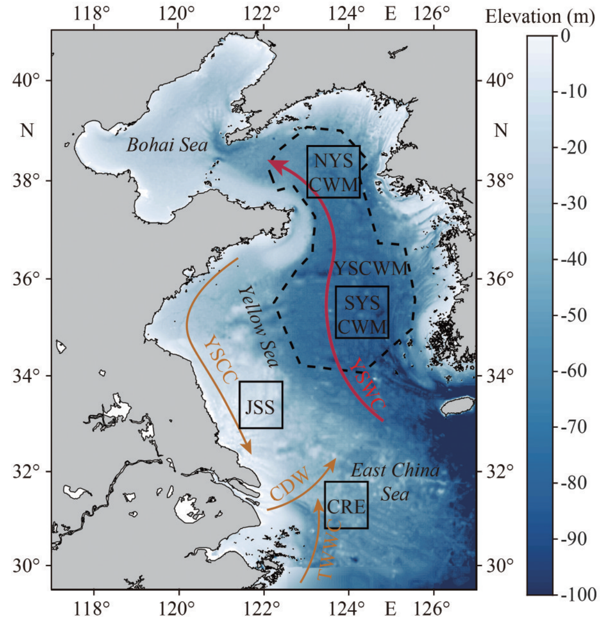

Fig.1 Study area and major oceanographic features

YSCWM: Yellow Sea Cold Water Mass; YSCC: Yellow Sea Coastal Current; YSWC: Yellow Sea Warm Current; CDW: Changjiang Diluted Water; TWC: Taiwan Warm Current; NYSCWM: Northern Yellow Sea Cold Water Mass; SYSCWM: Southern Yellow Sea Cold Water Mass; JSS: Jiangsu Shoal; CRE: Changjiang River estuary.

2.2 Dataset

2.2.1 In-situ data

The in-situ POC data used in this study were obtained from Guo et al. (2022). This dataset includes seven observational cruises conducted during 2017–2021, covering the entire YS and including all seasons of the year. Since this dataset lacks in-situ POC data from the Bohai Sea, the Bohai Sea was excluded from the study domain to ensure the accuracy of the research results. Details of each cruise are shown in Table 1.

2.2.2 Satellite remote sensing data

Monthly Level 3 MODIS-Aqua satellite datasets with a spatial resolution of 4 km×4 km were used to obtain chlorophyll-*a* (Chl-*a*) concentration, sea surface temperature (SST), photosynthetically available radiation (PAR), and remote sensing reflectance (R_{rs}) at 443, 490, 555, 645, 667, and 678 nm. The datasets were downloaded from the National Aeronautics and Space Administration (NASA) Ocean Biology Distributed Active Archive Center (https://oceancolor.gsfc.nasa.gov/l3/). Additionally, Suspended Matter (SPM) was calculated from monthly mean R_{rs} at 645, 667, and 678 nm using a semi-empirical radiative transfer (SERT) algorithm

Table 1 Summary of cruises in the YS during 2017–2021

Survey season	Survey date	Research vessel	Number of sampling stations
Winter	2017/12/18–2018/01/09	*Dongfanghong 2*	39
Spring	2018/03/28–2018/04/17	*Dongfanghong 2*	43
Summer	2018/07/24–2018/08/10	*Dongfanghong 2*	50
Autumn	2019/10/11–2019/10/18	*Lanhai 101*	35
Spring	2021/04/16–2021/04/27	*Lanhai 101*	52
Spring	2021/05/08–2021/05/19	*Lanhai 101*	47
Summer	2021/07/16–2021/07/28	*Lanhai 101*	50

proposed by Shen et al. (2014). Similarly, CDOM concentration was represented by the CDOM absorption coefficient at 355 nm (aCDOM (355)), derived from the exponential one-phase decay algorithm proposed by Mannino et al. (2008). The study spanned 2003–2023 to align with the complete time series of the MODIS-Aqua datasets and ensure temporal consistency across all ancillary products.

2.2.3 Reanalysis data

Monthly mean mixed layer depth (MLD) was obtained from the Oregon State University Ocean Productivity Data Set (http://sites.science.oregonstate.edu/ocean.productivity), with a spatial resolution of 1/12°×1/12° (approximately 9 km). Sea surface wind (SSW) speed was sourced from the ERA-5 reanalysis dataset provided by the European Centre for Medium-Range Weather Forecasts (ECMWF, https://cds.climate.copernicus.eu/), which was originally available at an hourly temporal resolution with a spatial resolution of 0.25°×0.25° and then aggregated into monthly means (Hersbach et al., 2020). Monthly sea surface salinity (SSS), nitrate, phosphate, dissolved oxygen (DO), and partial pressure of carbon dioxide ($p\mathrm{CO_2}$) data were taken from the Copernicus Marine Environment Monitoring Service (CMEMS, https://marine.copernicus.eu/). All ancillary fields were bilinearly regridded to a 4-km spatial resolution, consistent with that of the surface POC.

2.3 Method

2.3.1 Inversion algorithm

Two empirical algorithms were employed to estimate surface POC concentrations.

1. Normalized Difference Chlorophyll Index (NDCI) algorithm: This method utilizes the ratio of near-infrared to red spectral bands, which enhances the sensitivity to phytoplankton-derived particles. The algorithm is described by the following equations (Son et al., 2009):

$$N=(R_{\mathrm{rs}}(555)-R_{\mathrm{rs}}(443))/(R_{\mathrm{rs}}(555)+R_{\mathrm{rs}}(443)), \quad (1)$$

$$\log_{10}(\mathrm{POC})=a\times N^3+b\times N^2+c\times N+d, \quad (2)$$

where a, b, c, and d are the coefficients to be determined. In this formulation, N denotes the NDCI; $R_{\mathrm{rs}}(443)$ and $R_{\mathrm{rs}}(555)$ refer to the remote sensing reflectance at 443 nm (blue band) and 555 nm (green band), respectively. Specifically, the blue band is sensitive to phytoplankton pigment absorption, whereas the green band primarily reflects backscattering by suspended particulate matter.

2. Blue-green band ratio (BG) algorithm: a standard algorithm based on the NASA OceanColor protocols, which estimates POC using blue-green reflectance ratios (Stramski et al., 2008):

$$\mathrm{BG}=R_{\mathrm{rs}}(443)/R_{\mathrm{rs}}(555), \quad (3)$$

$$\mathrm{POC}=a\times(\mathrm{BG})^b, \quad (4)$$

where a and b are the coefficients to be determined. The spectral analysis focused on $R_{\mathrm{rs}}(443)$ and $R_{\mathrm{rs}}(555)$, representing blue and green band reflectance as defined previously.

2.3.2 Data interpolating empirical orthogonal function (DINEOF)

Satellite remote sensing datasets often exhibit gaps due to various factors such as cloud cover, sensor limitations, and challenges associated with atmospheric correction. This necessitates the use of effective interpolation techniques to ensure continuous spatial and temporal coverage. In this study, we applied the DINEOF approach, which iteratively reconstructs missing data by optimizing the number of EOF modes retained through cross-validation procedures (Beckers et al., 2006; Miles and He, 2010). DINEOF is effective at filling in missing data points according to existing data values, which makes the original and reconstructed datasets comparable.

2.3.3 Empirical orthogonal function (EOF) analysis

EOF analysis is a commonly used tool for data compression and dimensionality reduction in atmospheric, oceanic, and climate research (Preisendorfer, 1988). Given the presence of multi-source and non-stationary processes in the YS, EOF can identify dominant spatial patterns and their uncorrelated temporal coefficients. It not only clearly shows the coordinated variation relationship between surface POC and environmental factors, but also explains the seasonal-to-interannual distribution patterns and regional differences of surface POC more clearly. To better capture the interannual variation characteristics, we also calculated the monthly temporal coefficient series corresponding to each pattern.

2.3.4 Wavelet analysis

In four subregions (NYSCWM, SYSCWM, CRE, JSS), this study employs bivariate wavelet coherence (BWC) and the improved MWC to analyze time-localized, scale-specific coupling relationships. Specifically, BWC is used to identify the dominant coupling between POC and a single environmental factor, as well as their principal scales. MWC is applied to evaluate the scale dependence and gain effect of joint multi-factor impacts (Hu and Si, 2016; Xu et al., 2025). To focus on interannual-to-multiyear variability and avoid interference from seasonal signals, the diagnostic bandwidth is restricted to 17–85 months. Coherence strength is measured by coherence and the percent area of significant coherence (PASC). At the 95% significance level, an increase in PASC indicates a rise in explainable variation. In practical analysis, an added factor is considered to produce a significant gain when it increases PASC by ≥5%. The implementation of relevant analyses and significance assessment both follow the method of Hu and Si (2016).

3 RESULT

3.1 Algorithm performance

Figure 2a illustrates the correlation between in-situ POC concentrations and NDCI values, while Fig.2b presents the relationship between in-situ POC and the BG values. Both the NDCI and regional BG algorithms demonstrate reasonable performance in estimating surface POC concentrations.

Furthermore, POC data from the global BG algorithm were compared with those generated via the NDCI and regional BG algorithms. Detailed statistical validation was conducted to assess the retrieval performance of these three algorithms against in-situ observations, and the results were summarized in Fig.3a–c, namely the NDCI, regional BG, and global BG algorithms. Both the NDCI and regional BG algorithms exhibit similar performance in terms of mean absolute percentage deviation (MAPD) and root mean square error (RMSE). Notably, the regression slope associated with the NDCI algorithm is closest to the ideal value of 1, indicating higher fidelity and reliability in representing observed POC concentrations. While the regional BG algorithm yields a lower RMSE compared to the global BG algorithm, its coefficient of determination (R^2) is slightly lower, suggesting reduced explanatory power. This discrepancy implies that although regional BG reduces absolute prediction errors, it may capture less of the overall variability. In contrast, the NDCI algorithm consistently shows superior performance across both metrics. Error distribution histograms further support that both NDCI and regional BG algorithms

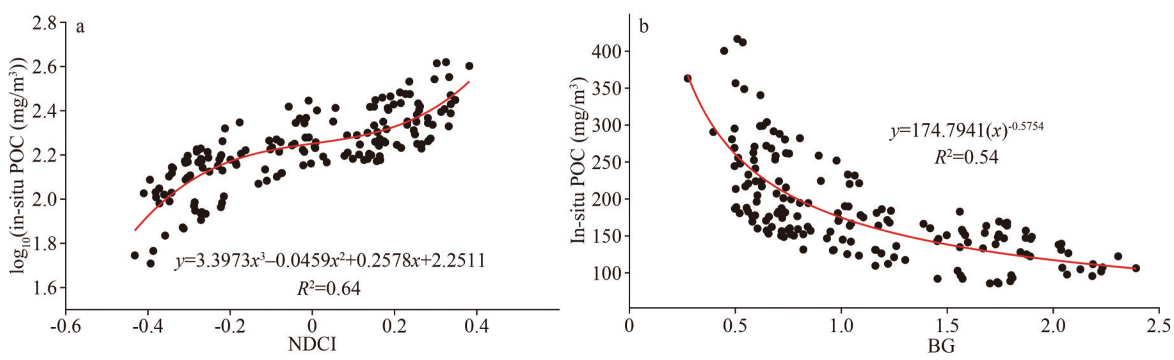

Fig.2 Relationships between in-situ particulate organic carbon (POC) concentrations and satellite-derived parameters

a. $\log_{10}$ transformed in-situ POC concentrations vs. NDCI (normalized difference chlorophyll index); b. in-situ POC concentration vs. BG ($R_{rs}(443)/R_{rs}(555)$). Black dots represent matched pairs of in-situ POC measurements and corresponding satellite-derived parameters used for model fitting, and red solid lines denote fitted regression curves. BG: blue-green band ratio; R^2: coefficient of determination.

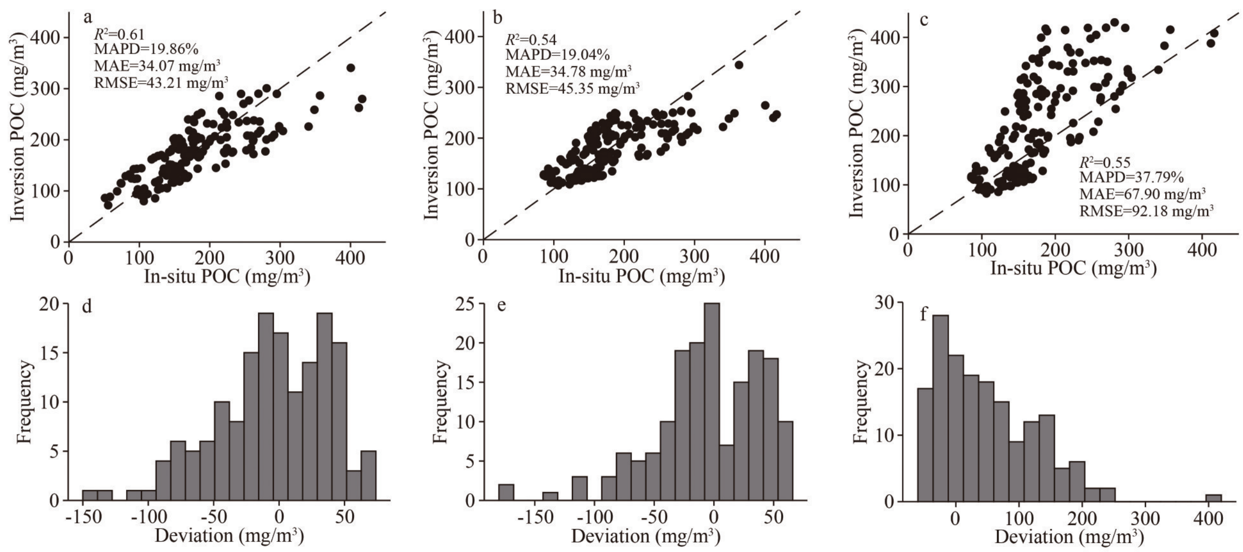

Fig.3 Validation results and error distributions of three particulate organic carbon (POC) inversion algorithms

a, d) NDCI algorithm; d, e. regional BG algorithm; c, f. global BG algorithm. MAE: mean absolute error; MAPD: mean absolute percentage deviation; RMSE: root mean square error; R^2: coefficient of determination.

reduce systematic biases relative to the global BG algorithm.

A threshold of 10 mg/L for SPM was adopted to distinguish between clear waters and turbid waters, consistent with the classification criteria in Wang et al. (2022). The results indicate that the NDCI algorithm shows lower error dispersion than the regional BG algorithm and significantly lower error than the global BG algorithm in both water types (Fig.4). Therefore, the NDCI POC data are used for all subsequent analyses in this study.

3.2 Spatiotemporal distribution of surface POC in the YS

Figure 5a shows the climatological spatial distribution of NDCI surface POC in the YS during 2003–2023, with concentrations ranging from 55.17 to 324.68 mg/m³ and a distinct spatial gradient observed. POC concentrations are relatively high in the northern YS and along the southern YS coastal waters, particularly in the Changjiang Diluted Water (CDW) area, while the central southern YS is characterized by the lowest POC values. Standard deviation analysis further reveals that the northern YS and central southern YS display relatively high variability (Fig.5b), whereas the coastal waters of the southern YS show low variability.

Surface POC in the YS exhibits distinct seasonal variations (Fig.6). For most regions of the YS, the seasonal variation follows a consistent pattern, with higher POC concentrations in late winter (Dec.) or early spring (Mar.) and lower concentrations in

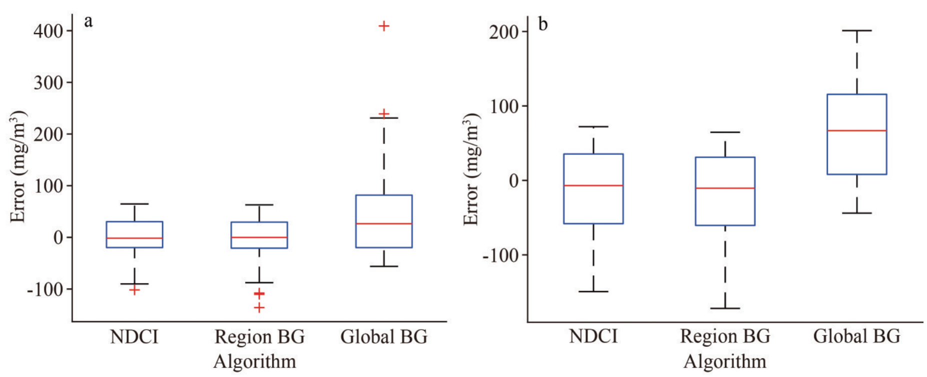

Fig.4 Comparison of error distributions among three algorithms in two type waters

a. clear waters; b. turbid waters. Blue boxes denote the interquartile range (IQR, between first and third quartiles). Red solid lines inside boxes are median values. Black dashed whiskers extend to data points within 1.5×IQR. Red plus symbols mark outliers (observations beyond the whiskers). NDCI: normalized difference chlorophyll index; BG: blue-green band ratio.

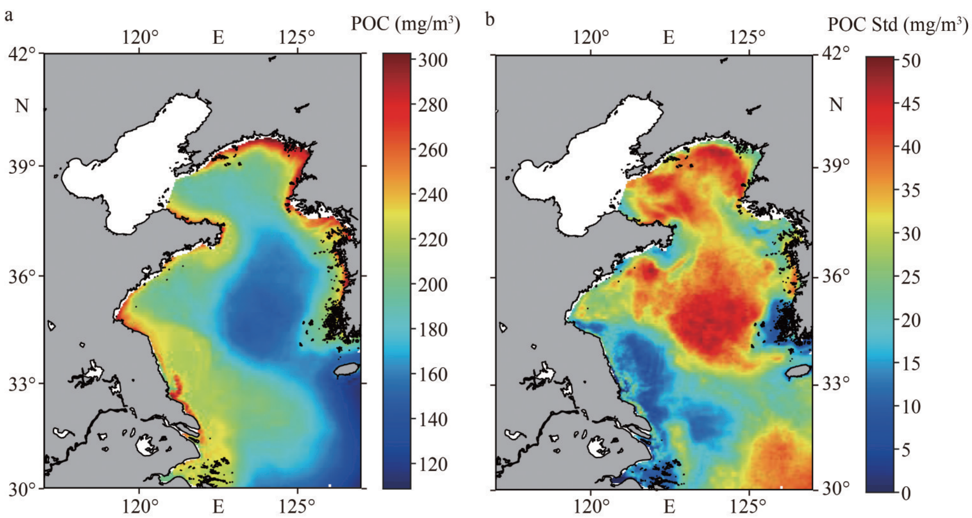

Fig.5 Spatial patterns of surface particulate organic carbon (POC) in the Yellow Sea (YS) during 2003–2023

a. climatological mean; b. standard deviation (Std).

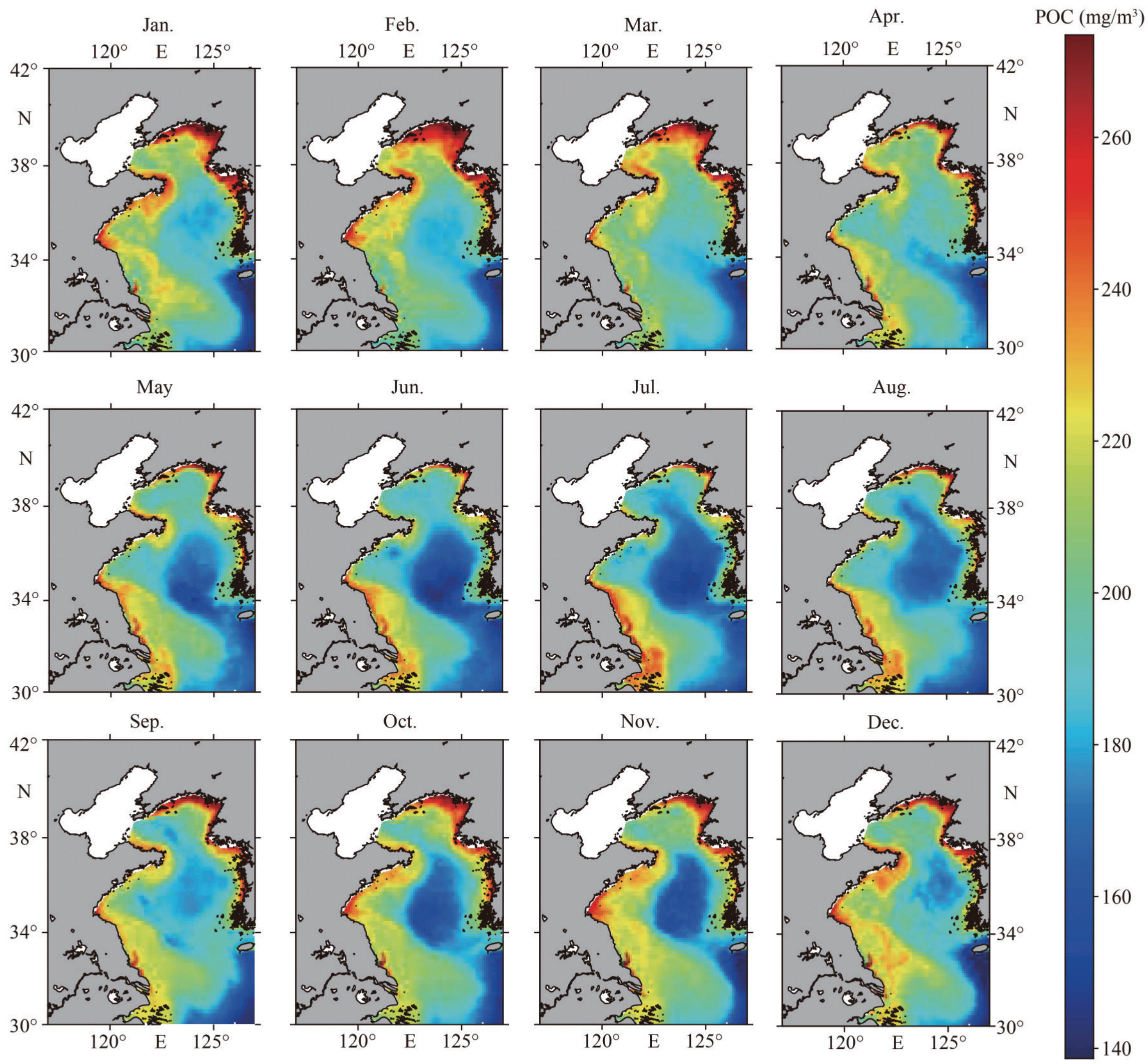

Fig.6 Spatial patterns of climatological monthly average surface particulate organic carbon (POC) in the Yellow Sea (YS)

summer (Jul.). Surface POC in the northern YS peaks around February, while that in the central southern YS mainly peaks in March–April. In contrast, the coastal waters in the southern YS display a distinct seasonal pattern, characterized by sustained high POC concentrations throughout the year and a summer peak. A special case is the CDW, where although surface POC concentrations reach their summer peak in July, the spatial extent of high-POC waters is relatively diminished.

EOF analysis of surface POC anomalies extracts two dominant and statistically significant modes (Fig.7). Specifically, the first mode (EOF1) explains 66% of the total variance, while the second mode (EOF2) accounts for 8% of the total variance. EOF1 exhibits a distinct coastal-offshore dipole spatial pattern, with positive values observed in the southern YS coastal waters and negative values dominating the northern YS and central southern YS (Fig.7a). EOF2 also presents a coastal-offshore dipole spatial pattern, featuring positive values along the northern YS coast and negative values in most other regions (Fig.7b). The time coefficient of EOF1 displays a pronounced seasonal cycle, with low values around February and high values in July-August, superimposed on an increasing trend in interannual fluctuations (Fig.7c & d). The time coefficient of EOF2 shows prominent fluctuations from late summer (July) to autumn, peaking in September, and features the largest fluctuation amplitude throughout the year (Fig.7c).

3.3 Long-term distribution trend of surface POC in typical subregions

The annual mean surface POC distribution shows statistically significant decreases ($P<0.05$) over time (Fig.8a), particularly in coastal and semi-enclosed subregions, except for areas directly influenced by offshore waters. Annual time series of these four subregions further highlight spatial heterogeneity in long-term POC trends (Fig.8b–e). Among the subregions, the SYSCWM and NYSCWM exhibit the strongest declining trends in surface POC concentration, with SYSCWM showing the most pronounced decrease. JSS also shows a significant downward trend, while the CRE displays a weak and statistically non-significant decrease (Fig.8b–e).

4 DISCUSSION

4.1 Main influencing factor of the spatiotemporal distribution patterns of surface POC

The time coefficient of EOF1 for surface POC displays a pronounced seasonal cycle, with minima occurring in winter and maxima in summer (Fig.7c–d). It is positively correlated with SST (R=0.88) and PAR (R=0.59), whereas it exhibits negative correlations with MLD (R=-0.72) and Chl *a* (R=

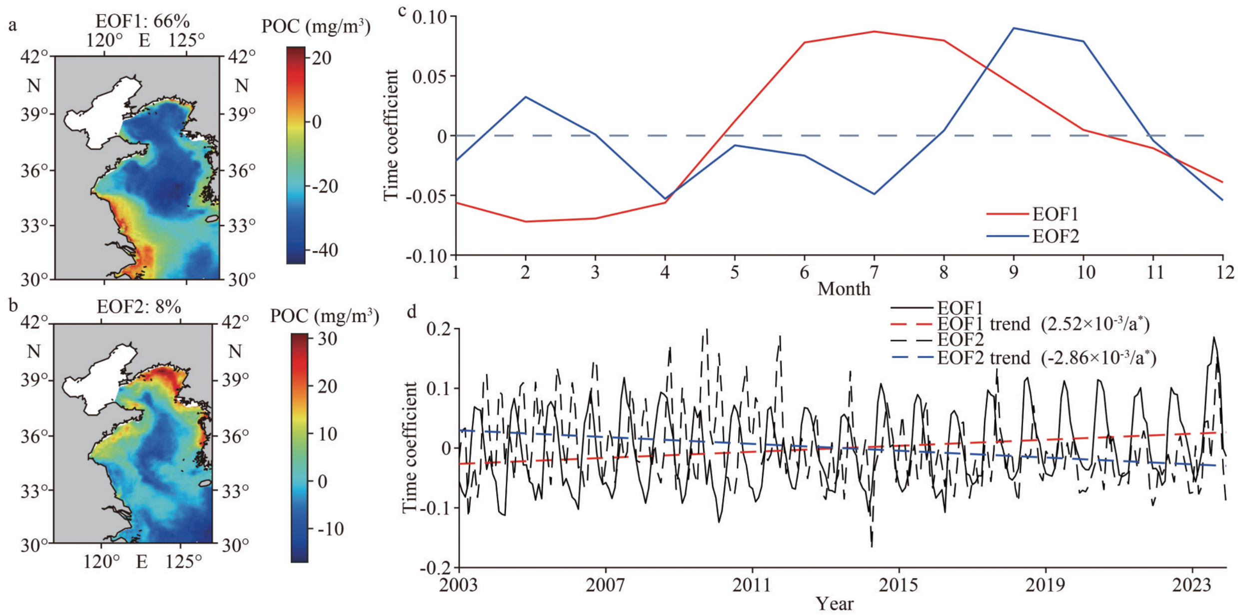

Fig.7 Dominant spatial-temporal modes of particulate organic carbon (POC) variability in the Yellow Sea (YS) derived from empirical orthogonal function (EOF) analysis

a. spatial patterns of the first EOF mode (EOF1); b. spatial patterns of the second EOF mode (EOF2); c. monthly mean time coefficients of EOF1 and EOF2; d. time coefficients of EOF1 and EOF2 during 2003–2023. * indicates a significant slope.

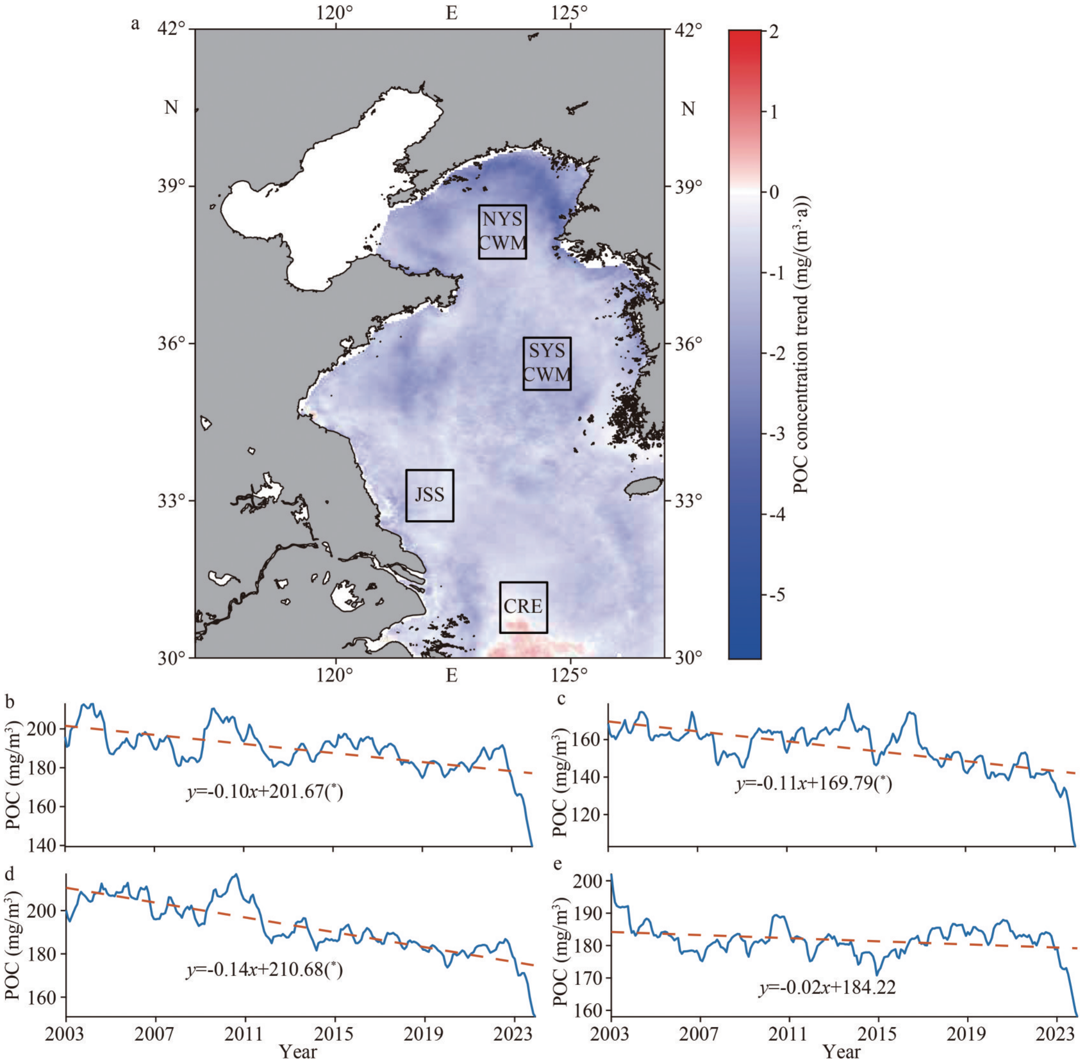

Fig.8 Trends of surface particulate organic carbon (POC) in the Yellow Sea (YS) during 2003–2023

a. spatial distribution of the linear trends of annual mean POC; b–e. regional time series with linear trends in the Northern Yellow Sea Cold Water Mass (NYSCWM) (b), Southern Yellow Sea Cold Water Mass (SYSCWM) (c), Jiangsu Shoal (JSS) (d), and Changjiang River estuary (CRE) (e). In panels (b–e), blue solid lines show the monthly mean POC time series, and orange dashed lines denote linear regression trends from annual means. * indicates a significant slope.

-0.76) (Table 2). These results demonstrate that the seasonal variability of surface POC is closely coupled to environmental parameters, among which SST, with the highest correlation coefficient, acts as the primary controlling factor. This finding is consistent with the established seasonal regulatory mechanism of surface POC, whereby POC dynamics are governed by cold, vertically mixed seawater in winter and warm, stratified seawater in summer (Fan et al., 2018; Ma et al., 2019).

Specifically, elevated SST in summer intensifies water column stratification, which suppresses the upward flux of nutrients from the benthic layer to the euphotic zone by reducing vertical mixing. This not only lowers Chl-*a* and POC concentrations in the surface layer but also accelerates the degradation and mineralization of the existing POC pool (Lao et al., 2023). In contrast, coastal waters influenced by plumes receive substantial terrigenous inputs (e.g., CDOM, SPM, and nutrients) during summer. Here, the synergistic effects of these optically active substances, nutrient-driven primary production, and sediment resuspension processes maintain high surface POC levels (Zhu et al., 2018; Chen et al., 2022; Ji et al., 2023).

The correlations between the EOF2 time coefficient and these environmental factors are weaker than those of EOF1 (Table 2). The spatial

Table 2 Correlations between environmental factors and surface particulate organic carbon (POC) time coefficients of EOF1 and EOF2

	EOF1	EOF2
	Temporal correlation	Temporal correlation
Chl *a*	-0.76**	-0.13**
SPM	-0.65**	0.06
SST	0.88**	0.13**
PAR	0.59**	-0.03
CDOM	-0.80**	-0.05
POC/Chl *a*	0.57**	0.18**
POC/SPM	0.27**	0.03
MLD	-0.72**	0
SSS	-0.83**	-0.12*
Nitrate	-0.20**	0.07
DO	-0.82**	-0.20**
$p\mathrm{CO_2}$	0.85**	0.05
Phosphate	-0.44**	-0.07
SSW	-0.18**	0.05

**, and * denote significance at the 0.01, and 0.05 levels, respectively. EOF: empirical orthogonal function; EOF1: the first EOF mode; EOF2: the second EOF mode; Chl *a*: chlorophyll *a*; SPM: suspended particulate matter; SST: sea surface temperature; PAR: photosynthetically active radiation; CDOM: colored dissolved organic matter; MLD: mixed layer depth; SSS: sea surface salinity; DO: dissolved oxygen; $p\mathrm{CO_2}$: partial pressure of carbon dioxide; SSW: sea surface wind.

pattern of EOF2 features positive values in the coastal waters of the northern YS, a distribution that aligns well with the occurrence of frontal and transition zones (Chen et al., 2022; Ji et al., 2023). Temporally, the EOF2 time coefficient exhibits a pronounced increasing trend from late summer to autumn (Fig.7c–d). These characteristics indicate that EOF2 variability is tied to local environmental gradient shifts and intermittent disturbances, rather than basin-scale integrated hydrological forcing. Consistent with previous studies on dynamical processes in the YS (Wei et al., 2020; Chen et al., 2022), these observations collectively demonstrate that EOF2 captures phase differences across the study domain instead of exerting basin-scale control, thus reflecting frontal-zone-dominated variability patterns.

4.2 Environmental control on interannual-to-multiyear variability of surface POC

To investigate variability on the interannual-to-multiyear timescale (17–85 months), we conducted a BWC analysis between surface POC and each environmental factor, using deseasonalized monthly anomaly data for the four subregions. The optimal environmental factor, defined by the highest coherence and PASC values for each subregion, is presented in Table 3. In the NYSCWM and JSS, surface POC exhibits significant in-phase coherence with CDOM at 60–85 months and 32–64 months, respectively (Fig.9a & c). Notably, CDOM slightly lags surface POC in NYSCWM. In the CRE, POC-CDOM coherence is concentrated at 16–32 months but displays spatial patchiness and temporal intermittency throughout the study period (Fig.9d). By contrast, surface POC in the SYSCWM shows significant out-of-phase coherence with SST at 64–85 months, with SST slightly leading POC during certain intervals (Fig.9b). These results demonstrate that CDOM (and SST in SYSCWM) is the optimal single factor explaining interannual-to-multiyear surface POC variability. This finding aligns with the role of CDOM in tracing particle supply and residence time, as well as SST in regulating water column stratification, mixing, and light conditions, all key drivers of surface POC dynamics (Seo et al., 2022; Hu et al., 2023; Yang et al., 2023).

To evaluate multi-factor controls, we calculated the MWCs between surface POC and two or more environmental factor combinations. Within the interannual-to-multiyear band (17–85 months), the covariability between POC and these factor combinations was summarized using coherence and PASC (Fig.10; Table 3). Additional factors are considered meaningful only when PASC increased by ≥5%. In NYSCWM, among all potential two-factor combinations, the CDOM+SSW exhibits the optimal performance in explaining surface POC variability at scales of 60–85 months, demonstrating the highest coherence and PASC. In the case of three-factor combinations, the increase in PASC is less than 5%; thus, no additional factors are retained. Consequently, the CDOM+SSW combination is identified as the optimal multi-factor combination for the NYSCWM.

In NYSCWM, JSS, and CRE, CDOM consistently dominates the optimal multi-factor combinations for surface POC. This indicates that riverine input serves as the primary controller of surface POC in these regions, with CDOM mediating the linkage between them (Su et al., 2017; Chen et al., 2022; Hu et al., 2023). However, differences in the auxiliary

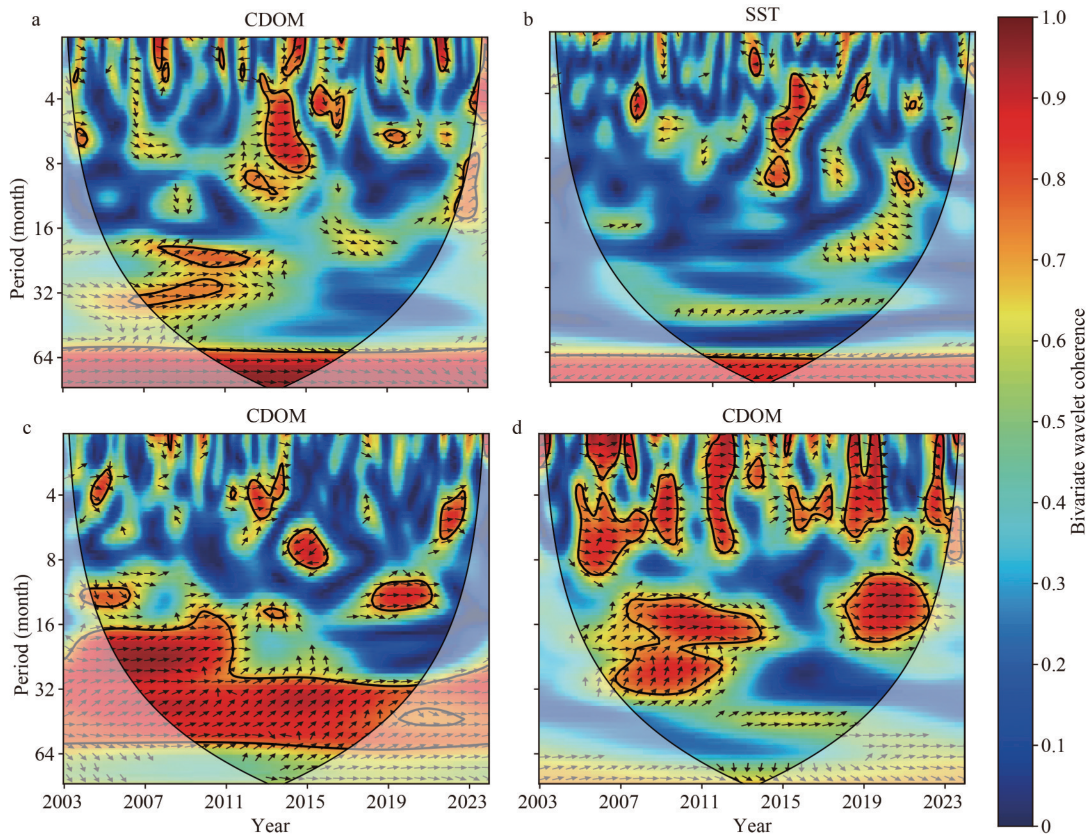

Fig.9 Optimal bivariate wavelet coherence (BWC) between the environmental factor and surface particulate organic carbon (POC) for the four subregions during 2003–2023

a. Northern Yellow Sea Cold Water Mass (NYSCWM); b. Southern Yellow Sea Cold Water Mass (SYSCWM); c. Jiangsu Shoal (JSS); d. Changjiang River estuary (CRE). Thick contours mark the 5% significance level against red noise. Pale areas show the cone of influence with possible edge effects. Colors represent wavelet coherency strength. Arrows indicate phase relationships: right (in-phase/positive correlation), left (anti-phase/negative correlation). CDOM: colored dissolved organic matter; SST: sea surface temperature.

components of their optimal multi-factor combinations reflect distinct regional environmental characteristics and regulatory mechanisms. The JSS is strongly influenced by combined wave-tidal resuspension (Su et al., 2017), which modulates SPM concentrations. Meanwhile, riverine-derived nutrients alter primary production, inducing variations in Chl *a* (Wei et al., 2018, 2020). These factors, together with CDOM, regulate POC dynamics. In the NYSCWM, SSW buffers terrestrial riverine POC input by regulating POC residence time (Hu et al., 2016, 2023; Xia et al., 2019), jointly maintaining stable POC dynamics with CDOM. In contrast, riverine input in the CRE is diluted by offshore water mixing, weakening terrigenous signals (Liu et al., 2016; Gao et al., 2020). SSS bridges this regulatory gap by reflecting the dilution intensity of the salinity front, synergizing with CDOM for POC regulation (Song et al., 2017). Despite CDOM's conserved regulatory role in these regions, these distinct processes lead to temporal-scale differences in POC variability. In SYSCWM, surface POC dynamics are governed by the YSCWM (Yu et al., 2022), with optimal regulators including Chl *a*, PAR, and pCO_2. The YSCWM modulates nutrient availability and light regimes, thus regulating these primary production-related factors and consequently governing surface POC production efficiency and accumulation (Fu et al., 2018; Seo et al., 2022; Guo et al., 2023; Yang et al., 2023).

5 CONCLUSION

Based on the model-derived surface POC data from 2003 to 2023, this study explored the seasonal variations, interannual-to-multiyear variations (17–85 months) of surface POC in the YS and its four subregions, as well as the corresponding regulatory mechanisms. The climatological mean surface POC exhibits a statistically significant decreasing trend in the entire YS, with obvious subregional variations.

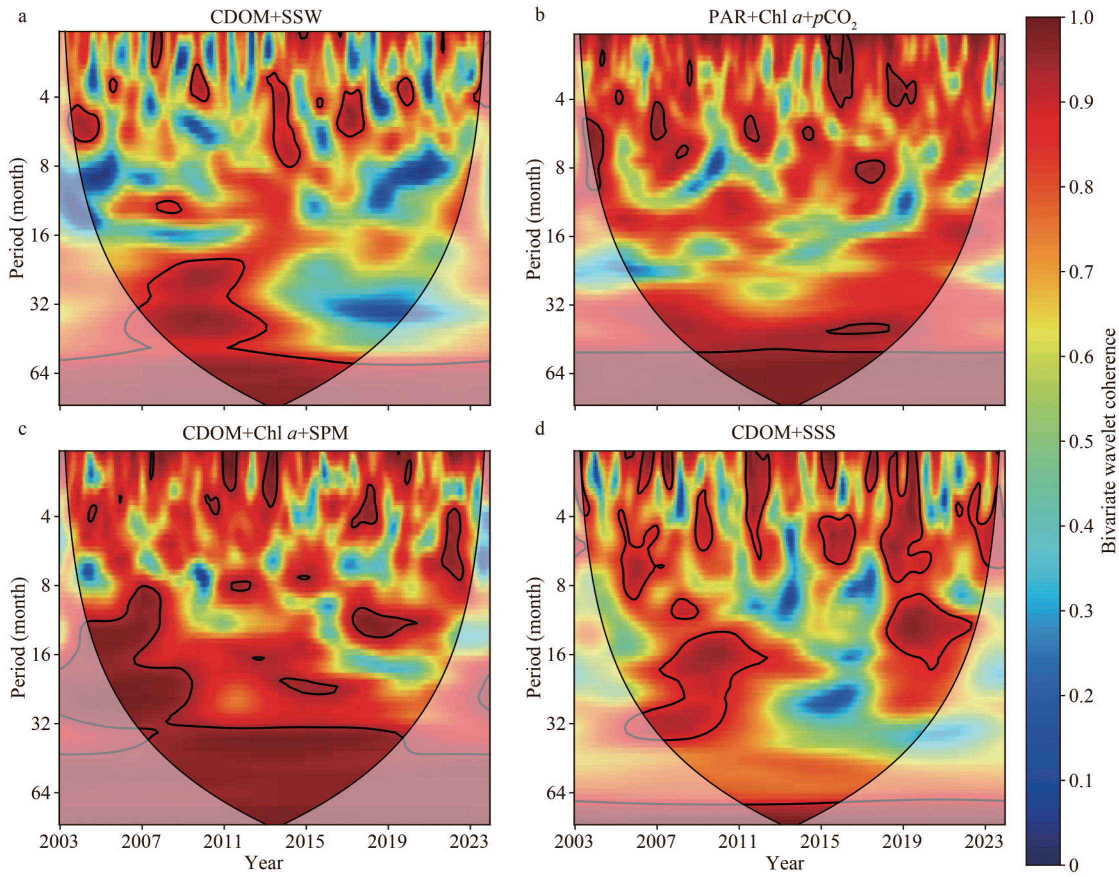

Fig.10 Multivariate wavelet coherence (MWC) of the best two- or three-factor combinations for surface particulate organic carbon (POC) variations for the four subregions during 2003–2023

a. Northern Yellow Sea Cold Water Mass (NYSCWM); b. Southern Yellow Sea Cold Water Mass (SYSCWM); c. Jiangsu Shoal (JSS); d. Changjiang River estuary (CRE). Thick contour lines denote 5% significance levels against red noise. Pale regions denote the cone of influence where edge effects might distort the results. The color denotes the strength of the wavelet coherence. CDOM: colored dissolved organic matter; SSW: sea surface wind; PAR: photosynthetically active radiation; $p\mathrm{CO_2}$: partial pressure of carbon dioxide; Chl *a*: chlorophyll *a*; SPM: suspended particulate matter; SSS: sea surface salinity.

Table 3 Coherence and PASC of the best multi-factor combinations for explaining surface POC variations in four subregions

Region	Number of variable	Best combination	BWC/MWC (%)	PASC (%)
NYSCWM	Single	CDOM	57.62	28.29
	Two	CDOM+SSW	76.40	40.53
SYSCWM	Single	SST	39.16	18.60
	Two	Chl *a*+$p\mathrm{CO_2}$	72.88	20.31
	Three	Chl *a*+$p\mathrm{CO_2}$+PAR	84.30	36.47
JSS	Single	CDOM	67.33	53.74
	Two	CDOM+Chl *a*	86.32	58.40
	Three	CDOM+Chl *a*+SPM	92.47	64.65
CRE	Single	CDOM	45.88	8.79
	Two	CDOM+SSS	73.44	23.41

NYSCWM: Northern Yellow Sea Cold Water Mass; SYSCWM: Southern Yellow Sea Cold Water Mass; JSS: Jiangsu Shoal; CRE: Changjiang River estuary; CDOM: colored dissolved organic matter; SSW: sea surface wind; SST: sea surface temperature; Chl *a*: chlorophyll *a*; $p\mathrm{CO_2}$: partial pressure of carbon dioxide; PAR: photosynthetically active radiation; SPM: suspended particulate matter; SSS: sea surface salinity; BWC: bivariate wavelet coherency; MWC: multivariate wavelet coherence; PASC: percent area of significant coherence.

This trend may reflect the differential responses of each subregion to global climate warming or human activities. At the seasonal scale, SST acts as the primary driving factor. Elevated summer SST intensifies water column stratification, which suppresses the upward flux of nutrients by reducing vertical mixing and consequently lowers surface POC concentrations. In contrast, summer coastal waters impacted by river plumes maintain high POC levels, sustained by substantial terrigenous inputs, coupled with in situ primary production and sediment resuspension processes.

At interannual-to-multiyear scales, CDOM is the optimal single factor controlling surface POC variations in three subregions (NYSCWM, JSS, and CRE), whereas SST serves as the optimal single factor in SYSCWM. Meanwhile, CDOM also dominates the optimal multi-factor combinations for surface POC in these three subregions. This indicates that riverine input is the primary controller of surface POC in these CDOM-dominated regions, with CDOM mediating the linkage between them. Differences in the auxiliary components of their optimal multi-factor combinations reflect distinct regional environmental characteristics and regulatory mechanisms. Specifically, the JSS is influenced by wave-tidal resuspension and changes in primary production driven by riverine nutrients. The NYSCWM is characterized by SSW buffering terrestrial riverine POC inputs. Riverine signals in the CRE are weakened by offshore mixing, with SSS supplementing the regulatory process. All these auxiliary factors synergize with CDOM to regulate surface POC. In SYSCWM, the YSCWM modulates environmental conditions related to primary production, thereby governing surface POC dynamics. These regional heterogeneities clarify the spatial differentiation of surface POC driving mechanisms in the Yellow Sea, providing a reliable scientific basis for accurate assessment of regional carbon budgets and optimization of marine numerical models.

6 DATA AVAILABILITY STATEMENT

Data will be made available on request.

References

Allison D B, Stramski D, Mitchell B G. 2010. Seasonal and interannual variability of particulate organic carbon within the Southern Ocean from satellite ocean color observations. *Journal of Geophysical Research*: *Oceans*, **115**(C6): C06002, https://doi.org/10.1029/2009JC005347.

Beckers J M, Barth A, Alvera-Azcárate A. 2006. DINEOF reconstruction of clouded images including error maps-application to the sea-surface temperature around Corsican island. *Ocean Science*, **2**(2): 183-199, https://doi.org/10.5194/os-2-183-2006.

Bridier G, Meziane T, Grall J et al. 2021. Sources, quality and transfers of organic matter in a highly-stratified sub-Arctic coastal system (Saint-Pierre-et-Miquelon, NW Atlantic). *Progress in Oceanography*, **190**: 102483, https://doi.org/10.1016/j.pocean.2020.102483.

Cai S B, Wu M, Le C F. 2022. Satellite observation of the long-term dynamics of particulate organic carbon in the East China Sea based on a hybrid algorithm. *Remote Sensing*, **14**(13): 3220, https://doi.org/10.3390/rs14133220.

Chen D X, Zeng L, Boot K et al. 2022. Satellite observed spatial and temporal variabilities of particulate organic carbon in the East China Sea. *Remote Sensing*, **14**(8): 1799, https://doi.org/10.3390/rs14081799.

Chen Z L, Yi Y B, Zhang H B et al. 2024. Differences in dissolved organic matter molecular composition along two plume trajectories from the Yangtze River Estuary to the East China Sea. *ACS Environmental Au*, **4**(1): 31-41, https://doi.org/10.1021/acsenvironau.3c00030.

Fan H, Wang X J, Zhang H B et al. 2018. Spatial and temporal variations of particulate organic carbon in the Yellow-Bohai Sea over 2002-2016. *Scientific Reports*, **8**(1): 7971, https://doi.org/10.1038/s41598-018-26373-w.

Friedlingstein P, Jones M W, O'Sullivan M et al. 2019. Global carbon budget 2019. *Earth System Science Data*, **11**(4): 1783-1838, https://doi.org/10.5194/essd-11-1783-2019.

Fu M Z, Sun P, Wang Z L et al. 2018. Structure, characteristics and possible formation mechanisms of the subsurface chlorophyll maximum in the Yellow Sea Cold Water Mass. *Continental Shelf Research*, **165**: 93-105, https://doi.org/10.1016/j.csr.2018.07.007.

Gao L, Gao Y Q, Song S Z et al. 2020. Non-conservative behavior of dissolved organic carbon in the Changjiang (Yangtze River) Estuary and the adjacent East China Sea. *Continental Shelf Research*, **197**: 104084, https://doi.org/10.1016/j.csr.2020.104084.

Guo C C, Yang S, Zhai W D et al. 2022. Biological-physical oceanographic coupling influencing particulate organic matter in the South Yellow Sea. *Frontiers in Marine Science*, **9**: 919423, https://doi.org/10.3389/fmars.2022.919423.

Guo J Q, Shen Y, Yuan H M et al. 2023. Bacterial reworking of particulate organic matter in a dynamic marginal sea: implications for carbon sequestration. *Organic Geochemistry*, **179**: 104583, https://doi.org/10.1016/j.orggeochem.2023.104583.

Heinze C, Meyer S, Goris N et al. 2015. The ocean carbon sink-impacts, vulnerabilities and challenges. *Earth System Dynamics*, **6**(1): 327-358, https://doi.org/10.5194/esd-6-327-2015.

Hersbach H, Bell B, Berrisford P et al. 2020. The ERA5 global reanalysis. *Quarterly Journal of the Royal Meteorological Society*, **146**(730): 1999-2049, https://doi.org/10.1002/qj.3803.

Hong Q Q, Peng S Y, Zhao D C et al. 2021. Cross-shelf export of particulate organic carbon in the northern South China Sea: insights from a ^{234}Th mass balance. *Progress in Oceanography*, **193**: 102532, https://doi.org/10.1016/j.pocean.2021.102532.

Honjo S, Eglinton T I, Taylor C D et al. 2014. Understanding the role of the biological pump in the global carbon cycle: an imperative for ocean science. *Oceanography*, **27**(3): 10-16, https://doi.org/10.5670/oceanog.2014.78.

Hu J W, Shi M C, Zhang T L et al. 2016. Evolution of Surface Cold Patches in the North Yellow Sea Based on Satellite SST Data. *Journal of Ocean University of China*, **15**(6): 936-946, https://doi.org/10.1007/s11802-016-3050-5.

Hu W, Si B C. 2016. Technical note: multiple wavelet coherence for untangling scale-specific and localized multivariate relationships in geosciences. *Hydrology and Earth System Sciences*, **20**(8): 3183-3191, https://doi.org/10.5194/hess-20-3183-2016.

Hu Y B, Yu F, Chen Z F et al. 2023. Two near-inertial peaks in antiphase controlled by stratification and tides in the Yellow Sea. *Frontiers in Marine Science*, **9**: 1081869, https://doi.org/10.3389/fmars.2022.1081869.

Ji C X, Yang G P, Chen Y et al. 2023. Contrast the distribution, transformation, and degradation of dissolved and particulate organic matter in the South Yellow Sea, the East China Sea, and its adjacent Kuroshio Current. *Marine Chemistry*, **248**: 104210, https://doi.org/10.1016/j.marchem.2023.104210.

Lao Q B, Chen F J, Jin G Z et al. 2023. Characteristics and mechanisms of typhoon-induced decomposition of organic matter and its implication for climate change. *Journal of Geophysical Research*: *Biogeosciences*, **128**(6): e2023JG007518, https://doi.org/10.1029/2023JG007518.

Li Z, Li S, Hu P et al. 2023. Improving storm surge simulations by considering wave-steepness-dependent drag coefficient in the northern East China Sea. *Ocean Modelling*, **186**: 102283, https://doi.org/10.1016/j.ocemod.2023.102283.

Liénart C, Savoye N, Bozec Y et al. 2017. Dynamics of particulate organic matter composition in coastal systems: a spatio-temporal study at multi-systems scale. *Progress in Oceanography*, **156**: 221-239, https://doi.org/10.1016/j.pocean.2017.03.001.

Liu S M, Qi X H, Li X N et al. 2016. Nutrient dynamics from the Changjiang (Yangtze River) estuary to the East China Sea. *Journal of Marine Systems*, **154**: 15-27, https://doi.org/10.1016/j.jmarsys.2015.05.010.

Ma W T, Xiu P, Chai F et al. 2019. Seasonal variability of the carbon export in the central South China Sea. *Ocean Dynamics*, **69**(8): 955-966, https://doi.org/10.1007/s10236-019-01286-y.

Mannino A, Russ M E, Hooker S B. 2008. Algorithm development and validation for satellite-derived distributions of DOC and CDOM in the U. S. Middle Atlantic Bight. *Journal of Geophysical Research*: *Oceans*, **113**(C7): C07051, https://doi.org/10.1029/2007JC004493.

Miles T N, He R Y. 2010. Temporal and spatial variability of Chl-*a* and SST on the South Atlantic Bight: revisiting with cloud-free reconstructions of MODIS satellite imagery. *Continental Shelf Research*, **30**(18): 1951-1962, https://doi.org/10.1016/j.csr.2010.08.016.

Preisendorfer R W. 1988. Principal Component Analysis in Meteorology and Oceanography. Elsevier, Amsterdam.

Rouf M A, Golder M R, Sumana Z A. 2021. Satellite-based observation of particulate organic carbon in the northern Bay of Bengal. *Environmental Advances*, **6**: 100124, https://doi.org/10.1016/j.envadv.2021.100124.

Seo J, Kim G, Hwang J. 2022. Sources and behavior of particulate organic carbon in the yellow sea and the East China Sea based on ^{13}C, ^{14}C, and ^{234}Th. *Frontiers in Marine Science*, **9**: 793556, https://doi.org/10.3389/fmars.2022.793556.

Shen F, Zhou Y X, Peng X Y et al. 2014. Satellite multi-sensor mapping of suspended particulate matter in turbid estuarine and coastal ocean, China. *International Journal of Remote Sensing*, **35**(11-12): 4173-4192, https://doi.org/10.1080/01431161.2014.916053.

Son Y B, Gardner W D, Mishonov A V et al. 2009. Multispectral remote-sensing algorithms for particulate organic carbon (POC): the Gulf of Mexico. *Remote Sensing of Environment*, **113**(1): 50-61, https://doi.org/10.1016/j.rse.2008.08.011.

Song G S, Li Y J, Hu S Z et al. 2017. Photobleaching of chromophoric dissolved organic matter (CDOM) in the Yangtze River estuary: kinetics and effects of temperature, pH, and salinity. *Environmental Science*: *Processes & Impacts*, **19**(6): 861-873, https://doi.org/10.1039/c6em00682e.

Stramska M, Bialogrodzka J. 2016. Satellite observations of seasonal and regional variability of particulate organic carbon concentration in the Barents Sea. *Oceanologia*, **58**(4): 249-263, https://doi.org/10.1016/j.oceano.2016.04.004.

Stramski D, Joshi I, Reynolds R A. 2022. Ocean color algorithms to estimate the concentration of particulate organic carbon in surface waters of the global ocean in support of a long-term data record from multiple satellite missions. *Remote Sensing of Environment*, **269**: 112776, https://doi.org/10.1016/j.rse.2021.112776.

Stramski D, Reynolds R A, Babin M et al. 2008. Relationships between the surface concentration of particulate organic carbon and optical properties in the eastern South Pacific and eastern Atlantic Oceans. *Biogeosciences*, **5**(1): 171-201, https://doi.org/10.5194/bg-5-171-2008.

Su M, Yao P, Wang Z B et al. 2017. Exploratory morphodynamic modeling of the evolution of the Jiangsu coast, China, since 1855: contributions of old Yellow River-derived sediment. *Marine Geology*, **390**: 306-320, https://doi.org/10.1016/j.margeo.2016.10.013.

Sun X S, Hu L M, Fan D J et al. 2024. Sediment resuspension accelerates the recycling of terrestrial organic carbon at a large river-coastal ocean interface. *Global Biogeochemical Cycles*, **38**(7): e2024GB008213, https://doi.org/10.1029/2024GB008213.

Tao S Q, Eglinton T I, Zhang L et al. 2018. Temporal variability in composition and fluxes of Yellow River particulate organic matter. *Limnology and Oceanography*, **63**(S1): S119-S141, https://doi.org/10.1002/lno.10727.

Wang S Q, Huan Y, Qiu Z F et al. 2016. Remote sensing of particle cross-sectional area in the Bohai Sea and Yellow Sea: algorithm development and application implications. *Remote Sensing*, **8**(10): 841, https://doi.org/10.3390/rs8100841.

Wang X, Wen Z D, Liu G et al. 2022. Remote estimates of total suspended matter in China's main estuaries using Landsat images and a weight random forest model. *ISPRS Journal of Photogrammetry and Remote Sensing*, **183**: 94-110, https://doi.org/10.1016/j.isprsjprs.2021.11.001.

Wang X J, Yu J, Fan H. 2020. Spatial and seasonal variability of surface particulate inorganic carbon and relationship with particulate organic carbon in the Yellow-Bohai Sea. *Journal of Oceanography*, **76**(5): 327-339, https://doi.org/10.1007/s10872-020-00547-5.

Wei Q S, Fu M Z, Sun J C et al. 2020. Seasonal physical fronts and associated biogeochemical-ecological effects off the Jiangsu Shoal in the Western Yellow Sea, China. *Journal of Geophysical Research*: *Oceans*, **125**(10): e2020JC016304, https://doi.org/10.1029/2020JC016304.

Wei Q S, Wang B D, Yao Q Z et al. 2018. Hydro-biogeochemical processes and their implications for *Ulva prolifera* blooms and expansion in the world's largest green tide occurrence region (Yellow Sea, China). *Science of the Total Environment*, **645**: 257-266, https://doi.org/10.1016/j.scitotenv.2018.07.067.

Wei X D, Shen F, Pan Y Q et al. 2019. Satellite observations of the diurnal dynamics of particulate organic carbon in optically complex coastal oceans: the continental shelf seas of China. *Journal of Geophysical Research*: *Oceans*, **124**(7): 4710-4726, https://doi.org/10.1029/2018JC014715.

Xia Y Y, Bao X W, Song D H et al. 2019. Tidal effects on the bottom thermal front of north yellow sea cold water mass near Zhangzi Island in Summer 2009. *Journal of Ocean University of China*, **18**(4): 751-760, https://doi.org/10.1007/s11802-019-3892-8.

Xu H B, Yang F C, Wang Y M et al. 2025. Comparative study of the variability of the phytoplankton biomass in two upwelling zones of the western Arabian Sea from 2003 to 2020. *Marine Pollution Bulletin*, **212**: 117522, https://doi.org/10.1016/j.marpolbul.2024.117522.

Yang J, Liu C L, Sun Q W et al. 2023. Interannual variability and long-term trends in intensity of the yellow sea cold water mass during 1993-2019. *Journal of Marine Science and Engineering*, **11**(10): 1888, https://doi.org/10.3390/jmse11101888.

Yu F, Ren Q, Diao X Y et al. 2022. The sandwich structure of the southern yellow sea cold water mass and yellow sea warm current. *Frontiers in Marine Science*, **8**: 767850, https://doi.org/10.3389/fmars.2021.767850.

Yu J, Wang X J, Fan H et al. 2019. Impacts of physical and biological processes on spatial and temporal variability of particulate organic carbon in the North Pacific Ocean during 2003-2017. *Scientific Reports*, **9**(1): 16493, https://doi.org/10.1038/s41598-019-53025-4.

Zhu W Z, Zhang H H, Zhang J et al. 2018. Seasonal variation in chromophoric dissolved organic matter and relationships among fluorescent components, absorption coefficients and dissolved organic carbon in the Bohai Sea, the Yellow Sea and the East China Sea. *Journal of Marine Systems*, **180**: 9-23, https://doi.org/10.1016/j.jmarsys.2017.12.003.